GLL
Geomatics, Landmanagement and Landscape No. 3 • 2025, 215–233

ISSN 2300-1496 https://doi.org/10.15576/GLL/211223

Research paper

Received: 1.09.2025
Accepted: 23.09.2025
Published: 15.11.2025

Multitemporal assessment of Krakow's urban microclimate (2002–2023) using satellite-derived land surface temperature, NDVI, and NDBI

Ewa Głowienka[1] 0000-0001-7326-1592
Zuzanna Micek[1]

[1] Department of Photogrammetry, Remote Sensing of Environment and Spatial Engineering, AGH University of Krakow
✉ Corresponding author: eglo@agh.edu.pl

Summary

Rapid urbanization has the potential to significantly alter local microclimates through the urban heat islands (UHI) effect. This study examines the spatial and temporal changes in land surface temperature (LST) in Krakow, Poland, from 2002 to 2023 in relation to changes in urban land cover. Multispectral satellite imagery from the Landsat 7/8/9 and Sentinel-2 missions (clear-sky August scenes at ~5-year intervals) was processed using Google Earth Engine to derive LST and spectral indices. The normalized difference vegetation index (NDVI) and normalized difference built-up index (NDBI) were computed to quantify vegetation loss and built-up area expansion, respectively. A supervised land cover classification (random forest) identified five classes – vegetation, water, built-up areas, roads, and bare soil – providing land cover maps for each analysis year. Satellite-derived LST was validated against in situ ground temperature measurements from 17 sensors deployed across the city in summer 2023. The results reveal pronounced surface warming in Krakow's urban core and in newly urbanized districts, corresponding to areas of intensive development and vegetation decline. Statistically, LST was negatively correlated with NDVI and positively correlated with NDBI, confirming that reduced green cover and increased impervious surfaces exacerbate surface heating. The satellite LST showed strong agreement with ground measurements, supporting the reliability of the remote sensing approach. Our integrated methodology and findings underscore the impact of urbanization on the city's microclimate and the critical role of green infrastructure in mitigating UHI effects. This approach provides a framework for evidence-based urban planning and climate adaptation strategies in other Central European cities.

Keywords

urban heat island • remote sensing • land surface temperature • NDVI • NDBI • Krakow

1. Introduction

Urban areas, as centers of intense economic and social activity, are increasingly affected by climate change and rapid land cover transformations. One of the most environmentally harmful phenomena in cities is the urban heat island (UHI) – a densely built-up area that exhibit higher air and surface temperatures than their rural surroundings. They are mainly caused by the replacement of natural vegetated surfaces with impervious materials (concrete, asphalt, roofing), which have high heat capacity and absorb and re-radiate solar energy. The reduction of vegetation and water surfaces removes natural cooling mechanisms, further intensifying urban warming. As a result, urban microclimates differ significantly from those of undeveloped areas, often to the detriment of thermal comfort and air quality for city residents [Santamouris 2015].

Krakow is the second largest and one of the most rapidly developing cities in Poland. Over the past two decades, the city has experienced dynamic urbanization, including expansion of residential districts, growth of transportation infrastructure, and development of industrial areas. These changes have turned large areas of permeable, vegetated land into built-up areas, which can disrupt the local heat balance and potentially amplify the UHI effect. Notably, new housing estates (e.g., Ruczaj and Mały Płaszów in the south) and major road projects (e.g., the Łagiewnicka Route and the northern bypass) were completed during the study period, confirming the broader intensification of urban land use. Krakow has a temperate transitional climate, with mean temperatures ranging from about –5°C in winter to 25°C in summer. This climatic setting, combined with the city's growth, makes Krakow a compelling case to investigate how urbanization influences microclimate. Indeed, urban expansion has been shown to increase the UHI intensity in cities around the world [Imhoff et al. 2010, Li et al. 2017].

Advances in Earth observation now enable detailed analysis of thermal patterns in cities. Satellite remote sensing provides systematic measurements of LST and land cover over large areas, which are invaluable for UHI studies. In particular, the Landsat program (with thermal infrared sensors on Landsat 7, 8, and 9) and the Sentinel-2 multispectral missions offer moderate-resolution imagery suitable for monitoring urban environmental changes. Derived spectral indices, such as the normalized difference vegetation index (NDVI) and the normalized difference built-up index (NDBI), allow quantitative assessment of changes in green cover and built infrastructure [Xue and Su 2017, Zha et al. 2003]. When combined with modern analytical tools and machine learning classification, these data can be used to map the spatial structure of the city and identify zones most susceptible to overheating [Chakraborty and Lee 2019].

The aim of this study is to perform an integrated assessment of Krakow's surface urban microclimate dynamics from 2002 to 2023 using multitemporal satellite data, and to validate the findings with ground-based measurements. LST analysis combined with land cover indices (NDVI, NDBI) and land use classification allows for quantitative determination of the impact of urbanisation on thermal patterns. The study also examines statistical relationships between LST and land cover indicators to elucidate how vegetation loss and built-up expansion contribute to the UHI effect. This work provides new insight into the extent of microclimate changes accompanying urban

growth in Central European cities and underlines the importance of integrating thermal remote sensing into urban planning for climate change adaptation.

2. Study area and methodology

Major processing steps (Fig. 1) include image acquisition in Google Earth Engine, spectral index calculation (NDVI, NDBI), supervised classification (random forest), land surface temperature (LST) retrieval using the mono-window algorithm, and validation with in situ measurements. Intermediate data products (maps of indices, classification, LST) were generated for each analysis year and compared to assess changes over time.

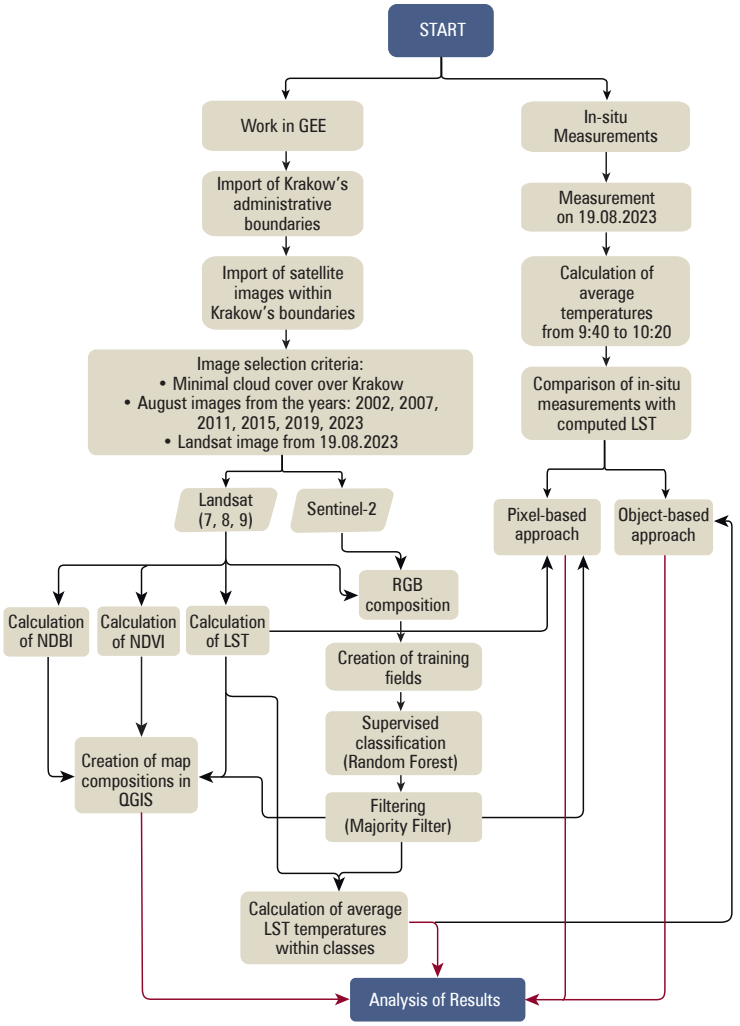

Source: Authors' own study

Fig. 1. Schematic flowchart of the analysis methodology.

2.1. Study area

Krakow, located in southern Poland (Fig. 2) covers ~327 km² and has a population of approximately 0.8 million. It is a historical city with a heterogeneous land use structure, including a dense urban core, extensive residential neighbourhoods, industrial zones (notably Nowa Huta in the east), as well as parks and river corridors along the Vistula. The city lies in a valley and is bordered by the Krakow-Częstochowa Upland to the north and Carpathian foothills to the south, which can influence local air circulation [Bokwa et al. 2015]. Krakow's climate is mid-latitude warm-temperate, with moderately cold winters and warm summers. Over the study period (2002–2023), the city underwent substantial urbanization, making it representative for analyzing UHI development in the region.

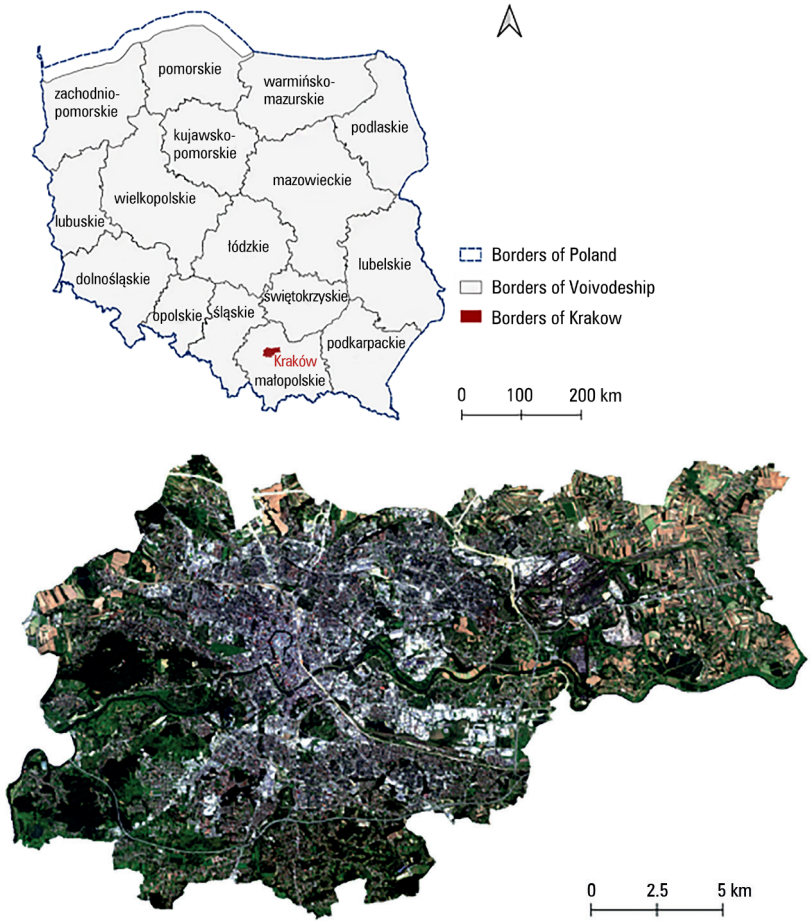

Source: Authors' own study

Fig. 2. Left: Poland with voivodeship boundaries; Krakow is indicated in red. Right: true-colour satellite mosaic of Krakow, clipped to the city's administrative boundary.

2.2. Data collection and processing

Multitemporal satellite data were the primary source for assessing land cover and surface temperature changes. We analyzed cloud-free summer imagery acquired in August of 2002, 2007, 2011, 2015, 2019, and 2023, at approximately 4–5 year intervals. This timing captures consistent seasonal conditions (peak solar heating and vegetation activity) for interannual comparison. We utilized images from Landsat 7 (Enhanced Thematic Mapper Plus, ETM+), Landsat 8 (Operational Land Imager/TIRS), Landsat 9 (OLI-2/TIRS-2), and Sentinel-2A/B (MultiSpectral Instrument) missions, which together provide continuous observations over the two-decade period. All satellite data were obtained and pre-processed via the Google Earth Engine [Gorelick et al. 2017] platform, using Level 2 products for Landsat (radiometrically and geometrically corrected) and surface reflectance products for Sentinel-2. Table 1 summarizes the key datasets and acquisition dates. An additional Sentinel-2 scene from 17 November 2024 was included to compare summer conditions with a cooler season and coincide with a late-season ground measurement campaign. Processing in the GEE environment ensured consistency and allowed multi-mission data to be integrated. Vector boundary data for Krakow (city administrative outline) and for Poland (for the overview map) were obtained from the Polish national geoportal, and used to clip the imagery to the extent of the city and for visualization.

Table 1. Satellite imagery datasets used for the analysis.

Date	Sensor	GEE dataset (ID)	Cloud cover [%]
17 Aug 2002	Landsat 7 ETM+	LANDSAT/LE07/C02/T1_L2	<5%
15 Aug 2007	Landsat 7 ETM+	LANDSAT/LE07/C02/T1_L2	<5%
26 Aug 2011	Landsat 7 ETM+	LANDSAT/LE07/C02/T1_L2	<5%
13 Aug 2015	Landsat 8 OLI/TIRS	LANDSAT/LC08/C02/T1_L2	<5%
24 Aug 2019	Landsat 8 OLI/TIRS	LANDSAT/LC08/C02/T1_L2	<5%
26 Aug 2019	Sentinel-2A MSI	COPERNICUS/S2_SR	<5%
19 Aug 2023	Landsat 8 OLI/TIRS	LANDSAT/LC08/C02/T1_L2	<5%
20 Aug 2023	Sentinel-2B MSI	COPERNICUS/S2_SR	<5%
17 Nov 2024	Sentinel-2A MSI	COPERNICUS/S2_SR	<10%

2.3. Land cover classification

A supervised land cover classification was performed for each reference year to evaluate changes in land use and relate them to temperature patterns. We used a random forest classifier (Breiman, 2001), implemented in GEE, applied to the multispectral satellite data. Five land cover classes were defined, capturing the dominant urban and environmental surfaces in Krakow: 1) vegetation (urban greenery, forests, lawns, agricultural fields), 2) water (rivers, reservoirs), 3) built-up areas (buildings and dense impervious surfaces), 4) roads (paved transportation surfaces), and 5) bare soil (open ground, construction sites, fallow land). Training data for the classifier was created by manual digitization of representative areas for each class on the composite true-colour imagery for each year. Approximately 50–100 training samples per class were identified across the city, covering different districts and including variations in appearance (for example, both high-density and suburban residential areas under 'built-up areas'). The classifier was then run on the full scene to produce a land cover map for each date. To reduce salt-and-pepper noise in the classification outputs, a majority filter (3×3 pixel moving window) was applied, generalizing isolated pixels to the predominant class of their neighbourhood. The random forest was configured with 100 trees. Other parameters were left at GEE defaults. For each classification, we retained about 20% of the digitized polygons as an independent validation set and computed confusion matrices. The resulting overall classification accuracies were above 85%, with Kappa coefficients around 0.8–0.9 for all years. Figure 1 provides a schematic of the processing workflow.

2.4. Spectral indices and retrieval of land surface temperature

Vegetation and urban built-up areas were quantified using NDVI and NDBI, respectively. These dimensionless indices (range –1 to +1) were calculated from the calibrated reflectance values of the imagery:

a. Normalized difference vegetation index (NDVI):

$$NDVI = (NIR - Red) / (NIR + Red) \quad (1)$$

where Red and NIR are the reflectances in the red (around 0.63–0.68 μm) and near-infrared (around 0.84–0.89 μm) bands [Tucker 1979, Xue and Su 2017]. NDVI is high for dense, healthy vegetation (approaching +1) and low or negative for non-vegetated surfaces. Water bodies typically yield NDVI ~ –0.3 or lower, bare soil and built-up areas around 0.0, sparse or stressed vegetation in the range 0.2–0.4, and very healthy green vegetation > 0.6. NDVI maps were produced for each year to identify changes in urban greenery and plant cover.

b. Normalized difference built-up index (NDBI):

$$NDBI = (SWIR - NIR) / (SWIR + NIR) \quad (2)$$

where SWIR is the reflectance in a short-wave infrared band (around 1.56–1.65 μm) and NIR is the near-infrared reflectance [Zha et al. 2003, He et al. 2010]. Built-up surfaces (concrete, asphalt) tend to reflect more in SWIR than in NIR, yielding positive NDBI values, whereas vegetated or wet surfaces give negative values. Thus, NDBI highlights urban fabric: values > 0 indicate impervious built surfaces, while values < 0 correspond to water, vegetation, or moist natural soils. NDBI was computed for each year to track the expansion of built-up land.

c. Land surface temperature (LST) represents the 'skin' temperature of the Earth's surface, as opposed to air temperature measured by standard meteorological instruments at 2 m height. Satellite thermal infrared data can be used to estimate LST remotely. In this study, we derived LST from Landsat thermal bands using a mono-window algorithm [Qin et al. 2001, Jiménez-Muñoz and Sobrino 2003], which corrects at-sensor brightness temperatures for emissivity and atmospheric effects in a simplified form. For each Landsat image (which provides a thermal band at 60 m resolution for Landsat 7 ETM+ and 100 m for Landsat 8/9 TIRS), the radiative transfer equation was inverted as:

$$LST = T_b / [1 + (\lambda \cdot T_b / c_2) \cdot \ln(\varepsilon)] - 273.15 \quad (3)$$

where T_b is the satellite-measured band brightness temperature (in Kelvin), λ is the thermal band wavelength, $c_2 = 1.438 \times 10^{-2}$ m · K (a constant derived from Planck's law), and ε is surface emissivity (unitless). Emissivity values (ε) were assigned based on land cover class. For instance, vegetated surfaces were set to ε ≈ 0.98, water ~0.99, and built-up areas (concrete/asphalt) ~0.94, following standard literature values [Snyder et al. 1998]. These ε estimates were applied to each pixel using the classified land cover maps to improve LST accuracy. The resulting LST maps (in °C) were then validated and analyzed for UHI patterns.

2.5. In situ temperature measurements

For validation, in situ ground temperature sensors were deployed across the city (at 17 locations) to collect temperature data from the surface (Fig. 3). On 19 August 2023, all the sensors (HOBO MX2300 series) were installed at representative sites (urban parks, residential blocks, industrial areas, etc.) to record surface-level temperature at 10-minute intervals. Clear-sky conditions prevailed with minimal wind, providing an opportunity to compare satellite-derived LST with ground observations under near-ideal UHI conditions. The average reading for each sensor between 09:40 and 11:20 AM local time was computed to coincide with the Landsat overpass (~11:00 AM). These averaged temperatures (ranging from ~24°C in parks to ~35°C in dense urban areas) serve as the ground truth for LST. The sensor data were then matched to the corresponding satellite pixel values for pixel-level validation and were also aggregated by land cover class for class-level validation. By examining errors and biases in these two ways, we assessed the reliability of the LST retrieval across different urban surface types.

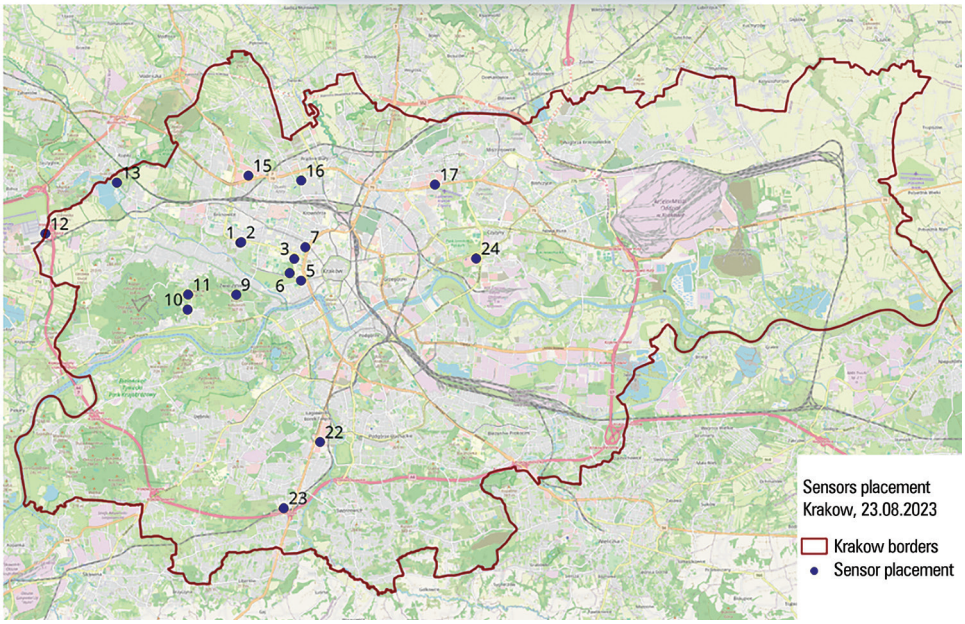

Source: Authors' own study

Fig. 3. Locations of ground temperature sensors deployed in Krakow on 19 August 2023 for LST validation (blue points).

3. Results

3.1. Land cover changes 2002–2023

Over the two decades, a substantial growth in built-up areas (gray) is evident, especially in the city outskirts and along new transportation corridors. New residential and commercial developments are visible in the northern and southern suburbs by 2023, compared to 2002. The urban core also became more consolidated, with previously open or vegetated parcels converted to impervious surfaces. Notably, the Nowa Huta district (north-east) saw expansion of industrial facilities, and sprawling development occurred in the southern districts. Vegetation (green) decreased in general, especially at the urban fringes, where farmland and grassland have been urbanized. Some large green spaces (e.g., parks and riverbanks) persisted within the city, but their proportional area declined relative to built-up land. The water class (blue, primarily the Vistula River and reservoirs) remained the same size. These classification outcomes indicate that changes in land use in Krakow between 2002 and 2023 were dominated by urban growth at the expense of vegetated land covers.

The classification accuracy was high for distinct classes like water and dense vegetation, while in some cases there was more confusion between built-up and bare soil or roads. The moderate spatial resolution of Landsat (30 m) made it challenging to

distinguish small features (e.g., narrow city streets or individual small buildings), leading to slight underestimation of the road class and some misclassification of scattered bare ground as built-up areas. Higher-resolution Sentinel-2 data from 2019 and 2023 provided more detail, refining the delineation of urban structures. Overall, the classified maps capture the major land cover transitions in Krakow, underscoring a clear intensification of urban land use. For example, the 2023 land cover map achieved an overall accuracy of ~89% (Kappa ~0.85); earlier years ranged from ~82–90% accuracy, confirming the robustness of the mapping.

3.2. Vegetation index (NDVI) trends

During the period under investigation, a noticeable decline in urban greenery was observed in many areas (Figure 4). In 2002, relatively high NDVI values not only appeared in parks and forests, but also in peri-urban zones that have since been developed. By 2023, the spatial extent of high-NDVI areas within the city had contracted, especially around the city periphery where new neighbourhoods were built. The city center and densely built districts consistently showed low NDVI (< 0.2) throughout the period, reflecting scant vegetation cover in those areas. One prominent pattern is the concentration of NDVI reduction in central Krakow: patches of vegetation within the inner city (e.g., around old fortifications or large estates) diminished as construction infill took place. Meanwhile, some outer areas that remained parkland or were afforested show stable or slightly increased NDVI (for instance, the restoration of vegetation in a former industrial site or improved urban green space management). The overall mean NDVI for the city dropped from approximately 0.36 in 2002 to 0.30 in 2023, indicating a net loss of healthy green cover. These changes confirm that urbanization has led to a measurable decrease in vegetative cover, which is a key factor in microclimatic regulation.

Quantitatively, the distribution of NDVI values shifted toward lower values over time. The histograms of NDVI (not included here) reveal that the proportion of pixels with NDVI > 0.5 (dense vegetation) declined markedly from 2002 to 2023, while the proportion of low NDVI (< 0.1) pixels increased, especially after 2011. This trend is consistent with the conversion of vegetated land to built-up surfaces. The loss of vegetation is expected to reduce evaporative cooling and shade, thereby contributing to higher surface temperatures locally.

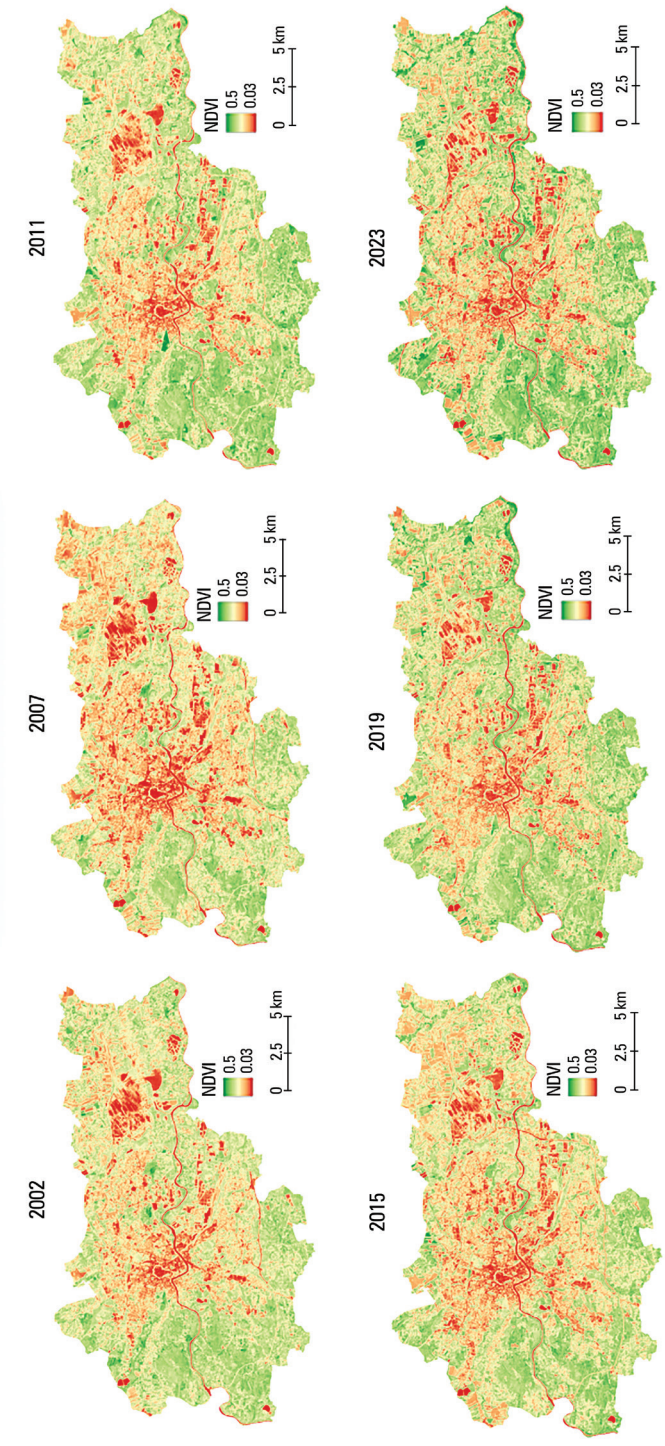

Source: Authors' own study

Fig. 4. NDVI maps of Krakow for the study years: a. 2002, b. 2007, c. 2011, d. 2015, e. 2019, f. 2023. High NDVI (green shades) indicates abundant healthy vegetation, while low NDVI (brown shades) indicates sparse vegetation or impervious surfaces.

3.3. Built-up index (NDBI) trends

The shift from 2002 to 2023 shows a clear increase in NDBI values across the city, reflecting urban expansion (Fig. 5). In 2002, areas with high NDBI were mainly confined within the historical center and industrial zones (e.g., Nowa Huta steelworks), with some moderate values along main roads. By 2023, the spatial extent and intensity of high-NDBI areas have grown substantially. Newly urbanized districts on the outskirts exhibit elevated NDBI, indicating the addition of large tracts of buildings and paved surfaces. For example, the northern and southern fringes of Krakow, which were semi-rural in 2002, show strong built-up signals by 2023 due to new housing and commercial developments. Inner-city areas that were partially vacant or undergoing redevelopment (e.g., post-industrial sites) also demonstrate high NDBI values.

Overall, the mean NDBI for Krakow increased from about –0.05 in 2002 to +0.15 in 2023, marking a significant rise in the built-up index (Fig. 5). The distribution of NDBI values shifted rightward: in 2002, the majority of the city's area had NDBI near zero or negative (signifying prevalent vegetation or bare soil), whereas by 2023 a much larger fraction of the city exhibited strongly positive NDBI values. This indicates that impervious surfaces became far more extensive. Such an increase in the built-up index is closely linked to higher heat retention and reduced evaporative cooling, which foreshadows greater surface warming in those areas.

3.4. Land surface temperature (LST) patterns

Figure 6 consists of LST maps of Krakow for the study years, revealing a general warming of the surface in many parts of the city between 2002 and 2023. Areas that experienced intensive development (high NDBI) correspond to emerging hotspots on the LST maps, whereas vegetated areas remained relatively cooler. In 2002, the highest LSTs were mainly confined to the dense urban core and large industrial complexes, but by 2023 many suburban zones that were urbanized also exhibited elevated LSTs. This spatial expansion of warm areas reflects the influence of urban growth on microclimate.

Statistically, we found that NDVI is inversely correlated with LST to a considerable degree, and NDBI is positively correlated. Districts with high average NDVI tend to be significantly cooler at the surface, consistent with the cooling effect of vegetation through shading and evapotranspiration. This mirrors the results of studies in other cities [Siddique et al. 2020, Lai et al. 2020] and global analyses [Peng et al. 2012] where higher NDVI is associated with lower LST. Conversely, we found a strong positive correlation between NDBI and LST ($r \approx +0.79$), indicating that built-up surfaces correspond to higher temperatures. Impervious materials store and re-radiate heat efficiently, so it is expected that as NDBI increases (suggesting more infrastructure), LST also increases. Our results align with those of recent studies in various climates. For instance, Shahfahad et al. [2023] reported that urban areas with greater built-up intensity exhibit higher land surface temperatures, and Afshari et al. [2025] documented divergent but generally positive relationships between developed land fractions and surface warmth across vegetation types.

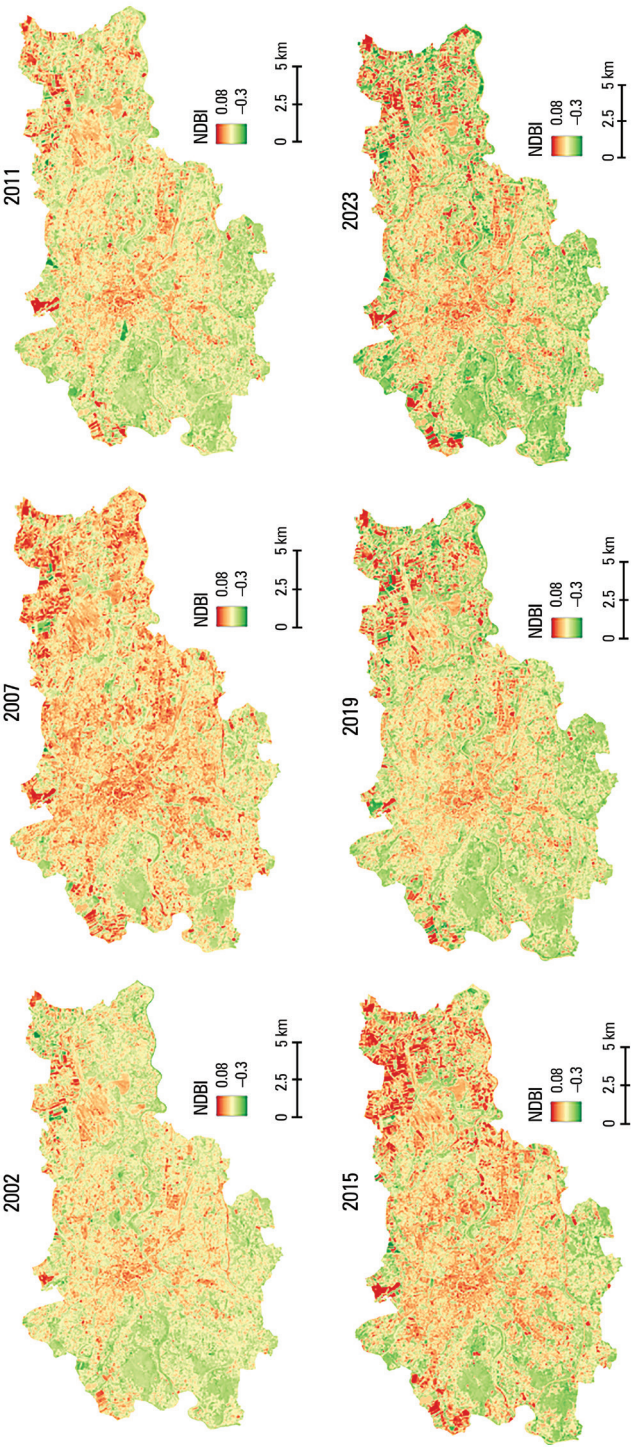

Source: Authors' own study

Fig. 5. NDBI maps of Krakow for: a. 2002, b. 2007, c. 2011, d. 2015, e. 2019, f. 2023. High NDBI (red shades) points to a strong built-up signal (extensive impervious surfaces), whereas low or negative NDBI (green shades) corresponds to non-built-up surfaces (vegetation, water).

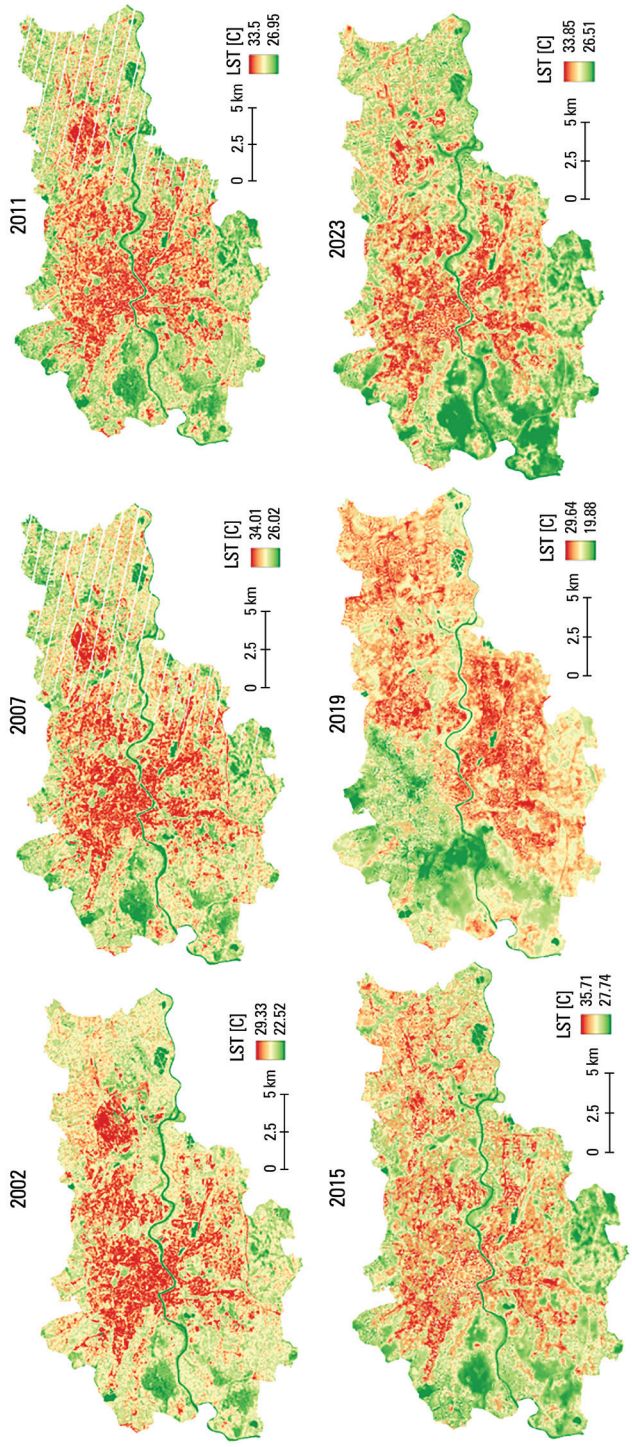

Source: Authors' own study

Fig. 6. Land Surface Temperature maps (in °C) of Krakow for: a. 2002, b. 2007, c. 2011, d. 2015, e. 2019, f. 2023, derived from Landsat thermal data. Each map represents LST around 10:00 AM local time on a clear summer day.

These correlations indicate that land cover composition is a key driver of Krakow's microclimate. The loss of vegetative cover (lower NDVI) and expansion of built-up surfaces (higher NDBI) together explain a significant portion of the spatial variance in LST observed within the city. In practical terms, this means that districts that experienced heavy urbanization not only show increased built-up index values but are also the hotspots in thermal maps, whereas the remaining green enclaves act as cooler patches. The statistical strength of these relationships (coefficients of determination on the order of R^2 ~0.65 for NDVI–LST and ~0.62 for NDBI–LST) confirms the critical role of land cover in shaping the UHI effect.

We evaluated the accuracy of the satellite LST estimates using the ground sensor measurements from 19 August 2023. Overall, the agreement between satellite and in situ temperatures was strong, with a coefficient of determination R^2 on the order of 0.85 and mean absolute differences of 2–3 °C. The validation was achieved in two ways: a) a pixel-based comparison – matching each sensor reading with the LST value of the corresponding pixel, and b) an object-based comparison – averaging sensor readings and LST over areas of a given land cover class.

For the pixel-based approach (17 points), linear regression indicated close correspondence, with most points falling near the 1:1 line. The largest discrepancies occurred at a few vegetated sites where the satellite LST was higher than the sensor measurement by 5–8°C. For example, in a park location the ground sensor recorded ~24.0°C while the satellite pixel (which integrates the canopy and ground surface heat) was ~30.0°C. In contrast, in the built-up locations the differences were smaller, typically within 3–4°C. These findings were reinforced by the class-based error analysis: built-up areas showed an average LST overestimation of +2.4°C (bias), with a root mean square error (RMSE) of ~4.1°C, whereas vegetation-dominated areas had a higher positive bias of +7–8°C in some cases (meaning the model over-predicted heating / under-predicted cooling), and an RMSE up to ~8.5°C for certain park pixels. Road surfaces had intermediate errors (bias ~1.9°C, RMSE ~7.6°C). The larger errors in densely vegetated and heterogeneous pixels suggest that factors like sub-pixel land cover heterogeneity, evaporative cooling, or canopy shading might not be fully captured by the simple mono-window model and emissivity assumptions. Still, the relatively low bias in green areas (+0.13°C on average) indicates that an average the LST model is quite adequate for those surfaces, while the positive biases in urban classes point to a slight systematic overestimation of surface heat in built-up environments.

In summary, the validation confirms that the remote sensing approach reliably captures the spatial pattern of LST across Krakow, showing strong correlation with measurements on the ground. Some overestimation in urban pixels may stem from the difference between surface temperature and air temperature measured by sensors, as well as the thermal inertia of building materials. Nevertheless, the magnitude of UHI signals (often on the order of 5–10°C differences between urban and rural areas) far exceeds the error margins. These results highlight that integrating satellite and ground observations is effective for monitoring urban thermal conditions, while also indicating areas for model refinement (such as incorporating more detailed emissivity or humidity corrections for vegetated surfaces).

4. Discussion

The findings of this study provide clear evidence that urbanization over the last two decades has had a measurable impact on Krakow's microclimate. The expansion of impervious built-up areas, coupled with the reduction and fragmentation of vegetated land, has intensified the urban heat island effect in the city. The multitemporal analysis showed that areas which underwent significant development – for example, new residential subdivisions or industrial parks – experienced increases in land surface temperature relative to their pre-urban state (Fig. 6). This outcome is in line with the fundamental understanding of UHI formation: replacing soil and vegetation with concrete and asphalt leads to greater solar energy absorption during the day and heat release at night, thus raising surface and near-surface air temperatures [Yang et al. 2016, Arnfield 2003]. Our Krakow case study corroborates results from other cities around the world that document similar trends. For instance, Bhattacharyya et al. [2025] demonstrated that rapid land cover change in Kolkata, India resulted in heightened thermal signatures, and Ullah et al. [2022] reported that urban sprawl in Tianjin, China caused a significant increase in UHI intensity. The consistency of our results with such global research highlights the universal nature of how urbanization affects microclimates.

A particularly noteworthy aspect is the strong inverse relationship between the presence of vegetation and surface heat. In Krakow, the districts with abundant greenery (parks, forests, riverbanks) function as cooler 'islands' within the urban fabric, alleviating extreme temperatures. This coincides with observations by Siddique et al. [2020] and Lai et al. [2020], who found that increases in NDVI are associated with decreases in LST in Beijing and Sardinian cities, respectively. The implication is that urban green infrastructure plays a critical mitigating role in the UHI effect. Our analysis quantifies this role in Krakow: areas of high NDVI (e.g., above 0.6) consistently showed LST several degrees lower than the city average. Conversely, high NDBI areas correspond to local hotspots. Maria et al. [2025] conducted a comparative microclimate study in a tropical city and arrived at a similar conclusion that industrial and densely built districts exhibit higher temperatures than residential or mixed-use areas, largely due to differences in surface materials and lack of vegetation. Our identification of Nowa Huta as one of the hottest zones in Krakow confirms those conclusions – industrial areas with sparse green cover create intense UHI conditions. Furthermore, Kamiński et al. [2025] found that in another Polish city, urban green spaces perceived as highly attractive by residents also had significantly lower surface temperatures and higher vegetation indices, pointing out that even informal 'wild' green spaces provide valuable cooling and ecosystem services.

The integration of supervised classification in our workflow allowed a closer examination of how specific land cover transitions contribute to warming. By categorizing land into classes, we could observe, for example, that the built-up class not only expanded in area but also showed the largest rise in average LST (from ~28°C in 2002 to ~33°C in 2023 in morning LST). On the other hand, the vegetated class, while shrinking in area, retained much lower average LST (~25°C in 2023). These class-based

differences highlight the heterogeneity of urban thermal behaviour and illustrate how targeted urban planning can make a difference. For instance, preserving green spaces within expanding neighbourhoods could help offset some of the heating caused by new development.

It is also important to note that UHI intensity can be exacerbated by extreme weather events. Recent research in Krakow has shown that heat waves combined with the UHI effect lead to significantly higher nocturnal temperatures and heat stress for residents [Hajto et al. 2025]. This proves that the microclimatic changes we observed are occurring in the context of broader climate trends and variability, which can amplify their impacts.

Despite these clear trends, some limitations of this study should be acknowledged. First, the moderate spatial resolution of the satellite data (30 m) and the focus on single summer days may not capture finer-scale microclimatic variations or seasonal differences in UHI intensity. The morning overpass time (~10–11 AM) means that our LST measurements likely underestimate the peak UHI intensity that manifests later in the afternoon or at night. Additionally, the simple mono-window model, while convenient, could be improved with more advanced algorithms or additional atmospheric data (e.g., a split-window approach or physics-based modelling) to reduce uncertainties. The largest LST residual errors were recorded for heterogeneous vegetated areas, indicating that variable emissivity and canopy shading can introduce uncertainty. Our in situ validation was limited to one clear summer day in 2023, and extending ground observations to multiple days or seasons (as done by Głowienka et al. [2025] with a multi-sensor harmonization approach) would provide a more robust evaluation. We also did not explicitly account for anthropogenic heat fluxes (e.g., from traffic or buildings), which can contribute to the UHI. Future work should address these limitations, for example by employing multi-sensor data harmonization techniques to enable consistent long-term monitoring and by modelling different urban development scenarios to test mitigation strategies.

5. Summary and conclusions

Urbanization has noticeably influenced Krakow's microclimate between 2002 and 2023. Multi-sensor satellite analysis reveals that the city's land surface has become warmer overall, with the most pronounced temperature increases occurring in areas of intensive development. Over two decades, Krakow saw a significant expansion of built-up areas (roads, buildings) accompanied by a loss of vegetation. These changes in land cover have led to an intensified UHI effect: daytime land surface temperatures in densely urbanized districts are now on average 8–10°C higher than in outlying rural areas, compared to a smaller difference at the beginning of the century. Areas with abundant vegetation (parks, riverbanks, forests) remain cooler, highlighting the vital cooling provided by urban green spaces.

The study found a strong inverse correlation between NDVI and LST and a strong direct correlation between NDBI and LST. This confirms that decreased vegetation

cover and increased impervious surfaces are driving forces of urban warming in Krakow. The supervised classification results further showed that the built-up class grew at the expense of greenery. Spatially, this translated into the expansion of hot zones and the reduction of cool zones on the thermal maps. The integration of in situ measurements validated the remote sensing results, with satellite-derived LST agreeing well with ground sensor data (within ~3°C on average). Some discrepancies in forested or grass-covered spots suggest that fine-scale factors (like shading or moisture) can modulate surface temperature beyond what the satellite captures, but these do not alter the broader findings.

In conclusion, the impact of urbanization on Krakow's microclimate is clearly evident in the satellite observations: urban growth has led to higher land surface temperatures and a stronger UHI. However, the pattern is not uniform as it depends on the land cover, which means that preserving and enhancing urban green infrastructure can significantly mitigate local heating. These insights are important for city planners and decision-makers. Adaptation measures such as creating new parks, planting street trees, installing green roofs, and using cooler (high-albedo) paving materials in construction could help reduce surface and air temperatures in the most affected neighbourhoods. The methodology applied in this research provides a repeatable framework for monitoring urban climate health and informing climate-sensitive urban planning. In the case of Krakow, maintaining a balance between development and natural environments will be crucial to ensure a resilient and liveable microclimate in the face of ongoing urban expansion and global climate change.

References

Afshari S., Shafiq M., Bahnarmand M., Alim M.A., Dewan A., Tang Z. 2025. Trend analysis and interactions between surface temperature and vegetation condition: divergent responses across vegetation types. Environmental Monitoring and Assessment, 197(3), 109–123. https://doi.org/10.1007/s10661-025-13729-9

Arnfield A.J. 2003. Two decades of urban climate research: a review of turbulence, exchanges of energy and water, and the urban heat island. International Journal of Climatology, 23(1), 1–26. https://doi.org/10.1002/joc.859

Bhattacharyya S., Ghosh S., Das P. 2025. Spatio-temporal influences of urban land cover changes on thermal-based environmental criticality and its prediction using CA-ANN model over Kolkata (India). Remote Sensing, 17(6), 1082. https://doi.org/10.3390/rs17061082

Bokwa A., Hajto M.J., Walawender J.P., Szymanowski M. 2015. Influence of diversified relief on the urban heat island in the city of Kraków, Poland. Theoretical and Applied Climatology, 122, 365–382. https://doi.org/10.1007/s00704-015-1577-9

Bowler D.E., Buyung-Ali L., Knight T.M., Pullin A.S. 2010. Urban greening to cool towns and cities: a systematic review of the empirical evidence. Landscape and Urban Planning, 97(3), 147–155. https://doi.org/10.1016/j.landurbplan.2010.05.006

Breiman L. 2001. Random forests. Machine Learning, 45(1), 5–32. https://doi.org/10.1023/A:1010933404324

Chakraborty T., Lee X. 2019. A simplified urban-extent algorithm to characterize surface urban heat islands on a global scale. Environmental Research Letters, 14(8), 084022. https://doi.org/10.1088/1748-9326/ab2fd8

Clinton N., Gong P. 2013. MODIS detected surface urban heat islands and sinks. Remote Sensing of Environment, 134, 294–304. https://doi.org/10.1016/j.rse.2013.03.008

Głowienka E., Malinverni E.S., Sanità M., Michałowska K., Kucza M. 2025. Harmonizing satellite thermal data with ground-based observations for climate long-term monitoring. International Archives of the Photogrammetry, Remote Sensing and Spatial Information Sciences, XLVIII-M-7-2025, 127–132. https://doi.org/10.5194/isprs-archives-XLVIII-M-7-2025-127-2025

Gorelick N., Hancher M., Dixon M., Ilyushchenko S., Thau D., Moore R. 2017. Google Earth Engine: planetary-scale geospatial analysis for everyone. Remote Sensing of Environment, 202, 18–27. https://doi.org/10.1016/j.rse.2017.06.031

Hajto M.J., Walawender J.P., Bokwa A., Szymanowski M. 2025. The impact of heat waves on diurnal variability and spatial structure of atmospheric and surface urban heat islands in Kraków, Poland. Sustainability, 17(7), 3117. https://doi.org/10.3390/su17073117

He C., Shi P., Xie D., Zhao Y. 2010. Improving the normalized difference built-up index to map urban built-up areas using a semiautomatic segmentation approach. Remote Sensing Letters, 1(4), 213–221. https://doi.org/10.1080/01431161.2010.481681

Imhoff M.L., Zhang P., Wolfe R.E., Bounoua L. 2010. Remote sensing of the urban heat island effect across biomes in the continental USA. Remote Sensing of Environment, 114(3), 504–513. https://doi.org/10.1016/j.rse.2009.10.008

Jiménez-Muñoz J.C., Sobrino J.A. 2003. A generalized single-channel method for retrieving land surface temperature from remote sensing data. Journal of Geophysical Research: Atmospheres, 108(D22), 4688. https://doi.org/10.1029/2003JD003480

Kamiński J., Głowienka E., Soszyński D., Trzaskowska E., Stuczyński T., Siebielec G., Poręba L. 2025. Integrating expert assessments and spectral methods to evaluate visual attractiveness and ecosystem services of urban informal green spaces in the context of climate adaptation. Sustainability, 17(4), 1349. https://doi.org/10.3390/su17041349

Lai S., Leone F., Zoppi C. 2020. Spatial distribution of surface temperature and land cover: a study concerning Sardinia, Italy. Sustainability, 12(8), 3186. https://doi.org/10.3390/su12083186

Li X., Zhou Y., Asrar G.R., Imhoff M.L., Li X. 2017. The surface urban heat island response to urban expansion: a panel analysis for the conterminous United States. Science of the Total Environment, 605–606, 426–435. https://doi.org/10.1016/j.scitotenv.2017.06.229

Maria A., Lopes A., Masiero É. 2025. Comparative study of microclimatic variables in industrial and residential areas of a tropical city using computational simulation and multivariate analysis. Theoretical and Applied Climatology, 156(1–2), 65–78. https://doi.org/10.1007/s00704-024-05283-0

Peng S., Piao S., Ciais P., Friedlingstein P., Ottlé C., Nan H., Zhou L., Myneni R.B. 2012. Surface urban heat island across 419 global big cities. Environmental Science & Technology, 46(2), 696–703. https://doi.org/10.1021/es2030438

Qin Z., Karnieli A., Berliner P. 2001. A mono-window algorithm for retrieving land surface temperature from Landsat TM data and its application to the Israel–Egypt border region. International Journal of Remote Sensing, 22(18), 3719–3746. https://doi.org/10.1080/01431160010006971

Santamouris M. 2015. Analyzing the heat island magnitude and characteristics in one hundred Asian and Australian cities and regions. Science of the Total Environment, 512–513, 582–598. https://doi.org/10.1016/j.scitotenv.2015.01.060

Shahfahad N., Bindajam A.A., Naikoo M.W., Horo J.P., Rahman A. 2023. Response of soil moisture and vegetation conditions in seasonal variation of land surface temperature and

surface urban heat island intensity in subtropical semi-arid cities. Theoretical and Applied Climatology, 153(1–2), 367–395. https://doi.org/10.1007/s00704-023-04477-2

Siddique M.A., Zhao C., Li H., Almazroui M. 2020. Assessment and simulation of land use and land cover change impacts on the land surface temperature of Chaoyang District in Beijing, China. PeerJ 8, e9115. https://doi.org/10.7717/peerj.9115

Snyder W.C., Wan Z., Zhang Y., Feng Y.-Z. 1998. Classification-based emissivity for land surface temperature measurement from space. International Journal of Remote Sensing, 19(14), 2753–2774. https://doi.org/10.1080/014311698214497

Tucker C.J. 1979. Red and photographic infrared linear combinations for monitoring vegetation. Remote Sensing of Environment, 8(2), 127–150. https://doi.org/10.1016/0034-4257(79)90013-0

Ullah N., Siddique M.A., Ding M., Grigoryan S., Zhang T., Hu Y. 2022. Spatiotemporal impact of urbanization on urban heat island and urban thermal field variance index of Tianjin City, China. Buildings, 12(4), 399. https://doi.org/10.3390/buildings12040399

Weng Q., Lu D., Schubring J. 2004. Estimation of land surface temperature – vegetation abundance relationship for urban heat island studies. Remote Sensing of Environment, 89(4), 467–483. https://doi.org/10.1016/j.rse.2003.11.005

Xue J., Su B. 2017. Significant remote sensing vegetation indices: a review of developments and applications. Journal of Sensors, Article ID 1353691. https://doi.org/10.1155/2017/1353691

Yang L., Qian F., Song D.-X., Zheng K.-J. 2016. Research on urban heat island effect: mechanisms and countermeasures. Procedia Engineering, 169, 11–18. https://doi.org/10.1016/j.proeng.2016.10.002

Zha Y., Gao J., Ni S. 2003. Use of normalized difference built-up index (NDBI) in automatically mapping urban areas from TM imagery. International Journal of Remote Sensing, 24(3), 583–594. https://doi.org/10.1080/01431160304987

Zhang X.Q. 2016. The trends, promises and challenges of urbanisation in the world. Habitat International, 54, 241–252. https://doi.org/10.1016/j.habitatint.2015.11.018